Applied Catalysis B: Environmental 202 (2017) 165–174

Contents lists available at ScienceDirect

Applied Catalysis B: Environmental

journal homepage: www.elsevier.com/locate/apcatb

Accelerated photocatalytic degradation of organic pollutant over metal-organic framework MIL-53(Fe) under visible LED light mediated by persulfate

Yaowen Gao[a,b], Simiao Li[a], Yixi Li[a], Linyu Yao[a], Hui Zhang[a,b,*]

[a] Department of Environmental Engineering, Wuhan University, Wuhan 430079, China
[b] Shenzhen Research Institute of Wuhan University, Shenzhen 518057, China

ARTICLE INFO

Article history:
Received 25 January 2016
Received in revised form 2 May 2016
Accepted 1 September 2016
Available online 1 September 2016

Keywords:
MOFs
Photocatalytic degradation
Visible LED light
Persulfate
Near-neutral pH

ABSTRACT

Photocatalysis based on metal-organic frameworks (MOFs) is being actively investigated as a potential technology in visible light harvesting and utilizing processes. Herein we report that MIL-53(Fe), an earth-abundant Fe-containing MOF material, shows photocatalytic activity for the degradation of Acid Orange 7 (AO7) from aqueous solution under visible LED light irradiation, yet the photocatalytic performance of bare MIL-53(Fe) was not satisfactory due to the fast recombination of photoinduced electron-hole pairs. This can be effectively overcome by adding the external electron acceptor (e.g., persulfate, PS) to the catalytic process. The accelerated photocatalytic degradation of AO7 is demonstrated by the result that the degradation efficiency of AO7 in the MIL-53(Fe)/PS/Vis process reached almost 100% within 90 min as compared to only 24% under the identical experimental conditions for the MIL-53(Fe)/Vis process. To investigate the mechanism of the MIL-53(Fe)/PS/Vis process, photoluminescence (PL) spectra, electrochemical measurements and electron paramagnetic resonance (EPR) analysis were performed. It was concluded that the efficient separation of photogenerated electrons and holes by the introduced PS and the subsequent formation of reactive radicals resulting from the activation of PS by photogenerated electrons accounted for the accelerated photocatalytic degradation of AO7 in the MIL-53(Fe)/PS/Vis process. Furthermore, the applicability of MIL-53(Fe) used in the persulfate-mediated photocatalytic process was systematically investigated in terms of the identification of reactive radicals, the reusability and stability of the photocatalyst, as well as the effect of operating parameters. The findings of this work highlighted the great potential of MOFs as photocatalysts and elucidated a new opportunity for persulfate remediation of contaminated water.

1. Introduction

Owing to the unlimited and sustainable energy influx from the Sun, photocatalysis using solar energy has been recognized as one of the most advantageous strategies to eliminate organic pollutants for relieving and resolving environmental issues facing mankind [1]. For the efficient utilization of sunlight, the development of visible-light-responsive photocatalysts is of great significance. Many metal oxides and sulfides such as WO_3 [2], CdS [3] and ZnS [4] can respond to visible light because the band gaps of these materials are generally narrower than those of TiO_2, which is only photoactive under ultraviolet (UV) light. Nevertheless, the easy agglomeration, difficult post-separation and low solar energy conversion efficiency of these inorganic catalysts hamper their large scale applications. Exploration of new catalysts has been attracting tremendous attention in the related research communities [5].

Metal-organic frameworks (MOFs), constructed from metal clusters interconnected by polydentate organic linkers, are a class of newly developed crystalline hybrid porous materials [6]. Their diverse structure features, such as large specific surface areas, uniform but tunable cavities and easily tailored chemistry, have endowed them with outstanding properties and potential applications in molecular sensing [7], gas storage [8], separation [9], and catalysis [10]. Very recently, MOFs have been identified to be capable of absorbing light upon irradiation, enabling them to be promising photocatalysts for a range of reactions [5,11]. Since the early report of photocatalytic activity in MOF-5 for phenol degradation under UV light irradiation [12], the application of MOFs as novel photocatalysts, particularly for the degradation of organic

* Corresponding author at: Department of Environmental Engineering, Wuhan University, Wuhan 430079, China.
E-mail address: eeng@whu.edu.cn (H. Zhang).

http://dx.doi.org/10.1016/j.apcatb.2016.09.005
0926-3373/

contaminants, has received considerable attention and become a hot research topic. For example, a double interpenetrated porous MOF $[Zn_4O(2,6\text{-ndc})_3(DMF)_{1.5}(H_2O)_{0.5}]\cdot 4DMF\cdot 7.5H_2O$ (UTSA-38) has been employed for the degradation of methyl orange (MO) in aqueous solution under UV or visible light illumination [13]. A UiO-66(NH_2) MOF has also exhibited visible-light-responsive photocatalytic activity toward degrading organic dyes [14].

Unfortunately, the relatively fast recombination of photogenerated electrons and holes leads to unsatisfactory photocatalytic efficiencies of the reported MOFs [15]. To date, many attempts have been paid to enhance the photocatalytic performance of photocatalysts by suppressing electron-hole recombination, such as doping and surface modification [16]. Among them, modification of single photocatalyst materials with metal or metal oxide nanoparticles (mostly noble metal or metal oxide) to form metal/MOFs heterostructured photocatalysts is a popular strategy [14,17,18], but the inevitable disadvantages of high price and limited abundance of noble metal restrict its practical application [15].

Alternatively, another important and feasible strategy to reduce charge carrier recombination probability is the addition of oxidants such as hydrogen peroxide (H_2O_2), persulfate (PS) and peroxymonosulfate (PMS) as electron acceptors to the photocatalytic reaction, owing to the immediate trapping of photogenerated electrons by the oxidants [19–21]. The work from Du et al. [22] was one of few attempts to introduce external electron acceptors to the MOF-based photocatalysis system, which confirmed that ammonium persulfate ($(NH_4)_2S_2O_8$) could be used as an efficient oxidant to enhance the photocatalytic property of MIL-53(Fe) photocatalyst for the decolorization of methylene blue (MB) under UV or visible light irradiation. However, $(NH_4)_2S_2O_8$ is rather unstable in the photocatalytic process and the detailed mechanism of the reaction is not clarified. Ai et al. [23] found that the introduced H_2O_2 could capture the photogenerated electrons in the conduction band of excited MIL-53(Fe) to form •OH radicals under visible light illumination, and thus facilitating the degradation of Rhodamine B (RhB). The amount of H_2O_2 added to the reaction was relatively high and the stability of MIL-53(Fe) in terms of iron leaching from the catalyst to aqueous phase under the experimental conditions was not yet demonstrated in the study. Although there have been some reports on the introduction of oxidants to MOF-based photocatalysis, the research work focusing on activation of PS by MOFs under visible light is rather scarce, especially using energy efficient light-emitting diodes (LEDs) as the irradiation source.

Herein we report the photocatalytic degradation of Acid Orange 7 (AO7) over MIL-53(Fe) under visible LED light irradiation at near-neutral pH (pH ~6.0). To accelerate the photocatalytic degradation of the dye over MIL-53(Fe), a more stable PS, namely sodium persulfate ($Na_2S_2O_8$), was added into the reaction. The reusability and stability of the photocatalyst was evaluated to assess its long-term applicability. Furthermore, the reactive radicals involved in the photocatalytic process were identified by electron paramagnetic resonance (EPR) technique and consequently a plausible reaction mechanism was proposed. Finally, the effect of several major factors on the photocatalytic degradation of AO7 was investigated.

2. Experimental

2.1. Chemicals

Iron chloride hexahydrate ($FeCl_3\cdot 6H_2O$), 1,4-benzenedicarboxylic acid (H_2BDC), dimethylformamide (DMF), $Na_2S_2O_8$ and AO7 were obtained from Sinopharm Chemical Reagent Co., Ltd. (Shanghai, China). Chitosan with a deacetylation degree of 91% was supplied by Yuhuan Ocean Biochemical Co., Ltd. (Zhejiang, China). The spin trapping agent 5,5-dimethyl-pyrroline-*N*-oxide (DMPO) was purchased from Aladdin, China. All chemicals employed in this work were of commercially available analytical grade and used without further purification. All the solutions were prepared with deionized water.

2.2. Preparation of MIL-53(Fe)

MIL-53(Fe) was synthesized via a facile solvothermal method using DMF as solvent [24]. Typically, a mixture of $FeCl_3\cdot 6H_2O$, H_2BDC and DMF with a molar ratio of 1:1:280 was stirred for 10 min at room temperature till a clear solution was formed. Then, the reactant mixture was transferred into a Teflon-lined stainless steel autoclave and heated at 150 °C for 15 h. After the heat treatment, the autoclave was allowed to cool naturally to room temperature, and the products were collected by filtration. To remove the solvent, the obtained yellow powder was re-heated at 150 °C in air overnight. After cooling down to room temperature, the solid was stirred for a few hours in a large volume of deionized water to extract the residual traces of DMF, and then filtrated and dried at 60 °C overnight.

2.3. Characterization of MIL-53(Fe)

X-ray diffraction (XRD) patterns were collected on a PANalytical X'Pert Pro X-ray diffractometer with Cu Kα radiation (λ = 1.5406 Å). Fourier transform infrared (FTIR) spectra on KBr pellets of the samples were recorded on a Nicolet FTIR 5700 spectrometer at a resolution of 4 cm^{-1}. The morphology of samples was observed with a Zeiss SIGMA field-emission scanning electron microscope (FESEM). The elemental composition of samples was characterized by energy-dispersive spectrometry (EDS) using an energy-dispersive X-ray spectrometer (Oxford INCA-400, UK). Surface electronic states were analyzed via X-ray photoelectron spectroscopy (XPS, ESCALAB 250Xi, USA). UV–vis diffuse reflectance spectra (UV–vis DRS) of the powder were obtained for the dry-pressed disk samples using a UV–vis spectrometer (UV-2550, Shimadzu, Japan). $BaSO_4$ was used as a reflectance standard in the UV–vis diffuse reflectance experiment. The photoluminescence (PL) spectra were obtained on a Hitachi F-4500 fluorescence spectrophotometer at an excitation wavelength of 340 nm. The photocurrent and Mott-Schottky measurements were conducted with a CS350 electrochemical workstation. The photoelectrodes were prepared according to the method reported by Zhao et al. but with a slight modification [25]. For the preparation of photoelectrodes, the photocatalysts were dispersed in chitosan solution to form a 10 mg mL^{-1} solution and ultrasonicated for 20 min. Then, 0.3 mL of colloidal solution was dip-coated on the indium doped tin oxide (ITO) surface and was allowed to dry in an oven at 60 °C for 2 h. The measurements were performed in a standard three-electrode system with the MIL-53(Fe) as working electrode, Pt wire as the counter electrode, saturated calomel electrode (SCE) as the reference electrode and 0.5 M Na_2SO_4 aqueous solution as the electrolyte. The LED lamps emitting white light were utilized as visible light source.

2.4. Photocatalytic activity evaluation and analyses

The photocatalytic degradation of AO7 was conducted in a Vis-LED photo-reactor, which was used in our previous work [26] and consisted of a 250-mL glass beaker with a 5-m flexible visible light LED strip containing white LED lamps wrapped around it at a distance of 5 cm (Fig. S1). The spectrum of LED lamps is shown in Fig. S2 and it is clear that the LED lamps emitted white light at 455 nm and further broadband Stokes-shift light emitted at roughly 500–600 nm. The irradiation intensity as measured by a digital lux meter (MS 6612, MASTECH, Shenzhen, China) was 0.47 mW cm^{-2}.

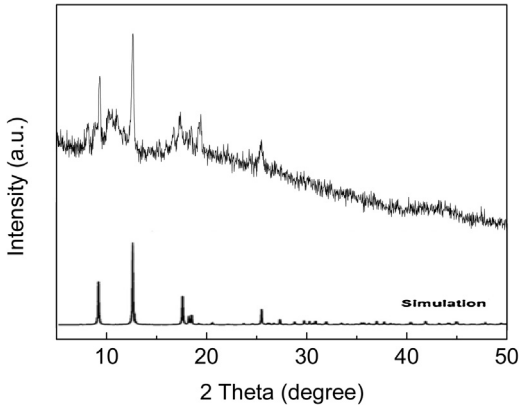

Fig. 1. XRD pattern of as-prepared MIL-53 (Fe).

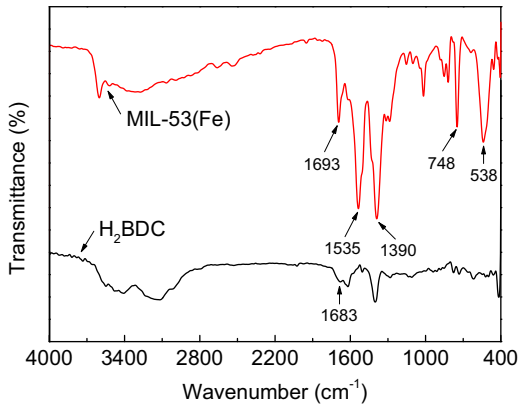

Fig. 2. FTIR spectra of MIL-53(Fe) and H_2BDC.

In addition, the photo-reactor was covered by a mirror to minimize the penetration of ambient light and the evaporation of water.

In each experiment, a 200-mL suspension containing AO7 (0.05 mM) and a desired amount of photocatalyst and PS was placed into the photo-reactor and then magnetically stirred at a constant speed, with the LED lamps being switched on simultaneously. At designated time intervals, aliquots of solution filtered using syringe membrane filters (0.45 μm) were analyzed on a UV–vis spectrometer (Rayleigh UV-9100) at the maximum wavelength of 485 nm.

The solution pH was measured with a combined glass electrode connected to a Mettler-Toledo FE20 pH meter. The concentration of residual PS was determined by an iodometric titration method [27] and the amount of leached iron ions was measured by spectrophotometry at λ = 510 nm after adding 1,10-phenanthroline to form an iron-phenanthroline complex [28]. The reactive radicals generated in the photocatalytic process were detected with a JEOL JES-FA200 spectrometer at room temperature.

3. Results and discussion

3.1. Characterizations

The XRD pattern of the prepared MIL-53(Fe) is shown in Fig. 1 and the appearance of appreciable sharp diffraction peaks demonstrated high quality of crystallinity in the photocatalyst, which accorded well with the previously reported MIL-53(Fe) as well as the simulated one [23,29]. To identify characteristic functional groups associated with MIL-53(Fe), the FTIR spectroscopy measurement was conducted. For comparison, the FTIR spectroscopy of organic linker (H_2BDC) was also performed. Fig. 2 shows the FTIR spectra of MIL-53(Fe) and H_2BDC and the spectrum of MIL-53(Fe) clearly exhibited the characteristic absorption peaks at 1693, 1535, 1390, 748 and 538 cm^{-1}. The absorption band at 1693 cm^{-1} corresponded to the stretching vibration of C=O bonds [23], whereas the one of pure ligand was noticed at 1683 cm^{-1}, indicating the absence of free ligand in MIL-53(Fe) [30]. The very strong peaks at 1535 and 1390 cm^{-1} were attributed to asymmetric and symmetric vibrations of carboxyl groups, respectively and this confirmed the presence of the dicarboxylate linker within the frameworks [15]. The band located at 748 cm^{-1} was due to C–H bending vibration of benzene ring in the organic linker [31,32]. Furthermore, the peak at 538 cm^{-1} was associated with the stretching vibration of Fe–O bonds [33], implying the formation of the Fe−oxo cluster between inorganic metal and the carboxylic group of organic linker.

Fig. 3 presents the SEM and the corresponding EDS images of MIL-53(Fe). As shown in Fig. 3a and b, MIL-53(Fe) displayed a rod-like structure, where the microrods had the width of 4–10 μm and the lengths of several tens of micrometers. This observation was similar to that of reported MIL-53(Fe) in the literatures [15,34]. In addition, the EDS elemental analysis shown in Fig. 3c revealed the presence of C, O and Fe elements in MIL-53(Fe). To confirm the elemental composition and to investigate the surface electronic states of MIL-53(Fe), XPS spectroscopy was further performed. Fig. 4 illustrates the XPS survey spectrum and the high-resolution XPS spectra of the photocatalyst. The XPS survey spectrum (Fig. 4a) verified that MIL-53(Fe) was composed only of C, O and Fe elements. The high resolution XPS C1s spectrum in Fig. 4b was fitted into two peaks with the binding energies at 284.8 and 288.7 eV, corresponding to the carbon components on the phenyl and the carboxylate groups of the organic linkers, respectively [35]. In the high resolution XPS O1s spectrum (Fig. 4c), the appearance of two peaks at 531.5 and 530.2 eV could be respectively attributed to the oxygen components on the organic linkers and the Fe–O bonds of MIL-53(Fe) [30,36]. For the high resolution XPS spectrum of Fe2p (Fig. 4d), the two peaks around binding energy of 711.5 and 725.4 eV were ascribed to Fe $2p_{3/2}$ and Fe $2p_{1/2}$ respectively and were characteristic of Fe(III) in MIL-53(Fe) [22]. Together with the above characterization results, it can be inferred that the MIL-53(Fe) photocatalyst has been synthesized successfully.

The light-absorption property of MIL-53(Fe) was explored through the UV–vis DRS measurement and the corresponding results are depicted in Fig. 5. As shown in Fig. 5a, H_2BDC had no optical response in the visible light region; on the contrary, MIL-53(Fe) displayed a strong absorption within the visible light range, signifying its potential capacity for visible-light harvesting. In the UV–vis DRS spectrum of MIL-53(Fe), the band centered at 440 nm was attributed to the spin-allowed d−d transition ($[^6A_{1g} \rightarrow {}^4A_{1g} + {}^4Eg(G)]$) of Fe^{3+} in MOFs [37,38]. The band gap energy of a semiconductor catalyst was an important optical property parameter for evaluation of the formation and transfer of photoinduced electrons and holes [39]. The optical band gap of MIL-53(Fe) could be calculated according to the energy dependence relation of $\alpha h\nu = A(h\nu - E_g)^{n/2}$, where α, h, ν, E_g and A are absorption coefficient, Plank constant, light frequency, optical band gap and a constant, respectively and n is determined by the type of optical transition in the semiconductor ($n = 1$ for a direct transition) [40]. The band gap energy of MIL-53(Fe) was estimated from a plot of $(\alpha h\nu)^2$ as a function of the photo energy ($h\nu$) to be 2.62 eV (Fig. 5b), which was close to the data previously reported for MIL-53(Fe) (2.72 eV) [30]. Therefore, the potential photoreactivity of MIL-53(Fe) could be expected, attributing to its prominent optical property in the visible light region.

3.2. Photocatalytic activity of MIL-53(Fe)

The photocatalytic degradation of refractory organic pollutants in aqueous solution is of great importance in many fields and

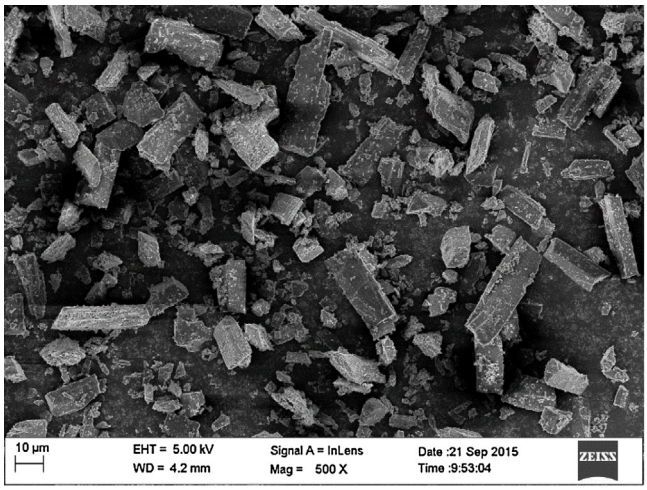

(a)

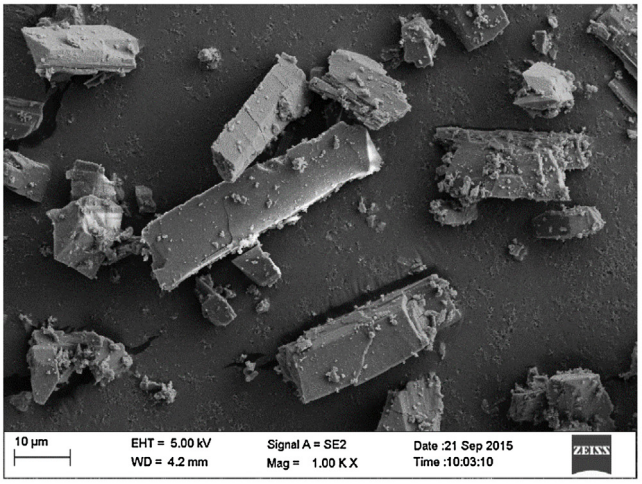

(b)

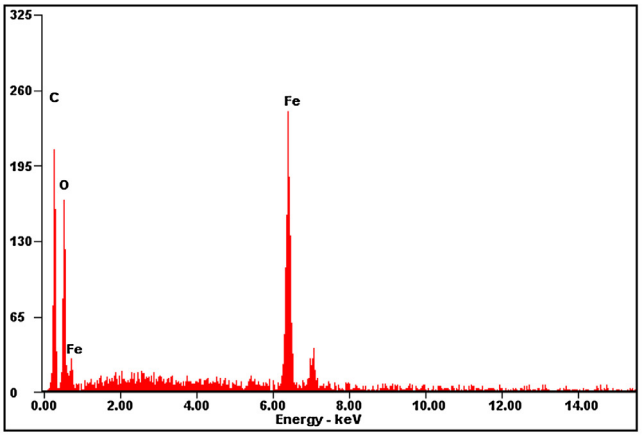

(c)

Fig. 3. SEM and the corresponding EDS images of MIL-53(Fe) (500× for (a), 1000× for (b)).

provides a common way to examine potential catalytic activity of photocatalysts [41]. Following most of the previous works, the organic dye AO7 was selected as probe to assess photocatalytic activity of MIL-53(Fe), for it was convenient to monitor dye decolorization using UV–vis absorption spectroscopy.

Fig. 6 represents the variation of AO7 concentration (C/C_0) as a function of reaction time in various catalytic processes. In the absence of photocatalyst, no significant decolorization of AO7 was noted after visible light irradiation for 90 min, reflecting that AO7 was quite stable toward incident light. The negligible removal of AO7 in the PS/dark or PS/Vis process revealed that PS could neither decolorize AO7 directly nor be activated by visible light. With bare MIL-53(Fe) as the catalyst, approximately 10% of AO7 was removed within 90 min, probably due to the adsorption of the catalyst. Considering that iron-based catalyst might activate PS in the catalytic process, the control experiment was further performed in the presence of PS and MIL-53(Fe) in the dark, where the bleaching degree of AO7 was about 17%, suggesting that MIL-53(Fe) exhibited potential capacity toward the activation of PS. While in the presence of visible light illumination, MIL-53(Fe) showed moderate photocatalytic activity without PS, and about 24% removal of AO7 was achieved. This could be mainly attributed to the generation of reactive charge carriers from the visible-light-illuminated MIL-53(Fe); however, the removal efficiency of AO7 was unsatisfactory, which might be ascribed to the fast recombination of photogenerated electrons and holes [22]. Intriguingly, the introduction of PS could significantly enhance the photocatalytic performance of MIL-53(Fe), and AO7 was nearly completely decolorized within 90 min in the MIL-53(Fe)/PS/Vis process with 82% of PS being decomposed simultaneously (Fig. S3).

The superior performance of the MIL-53(Fe)/PS/Vis process for the decolorization of AO7 could be evidenced by the time-dependent UV–vis absorption spectra. As shown in Fig. 7a, for AO7 solution before reaction, there was a main band in the visible region located at 485 nm, which accounted for the orange color of the solution and could be attributed to the azo linkage [42]. Meanwhile, the two other absorption bands at 310 and 229 nm in the UV region were associated with the naphthalene and benzene rings, respectively [43,44]. As the reaction proceeded, the visible band of the dye decreased gradually and finally disappeared, indicating the fragmentation of its chromophoric structure in the vicinity of the azo-linkage by oxidation. At the same time, the decay of the band at 310 nm was also observed, attributing to the opening of the naphthalene ring [20]. In addition, the absorbance at 229 nm increased and reached maximum at 20 min, and then decreased gradually with the irradiation time. This change could be reasonably assigned to the formation and degradation of benzene type intermediates.

In order to confirm the formation of the oxidation intermediates in the MIL-53(Fe)/PS/Vis process, FTIR spectra in the photocatalytic degradation of AO7 were recorded as a function of irradiation time. From Fig. 7b, it is clearly seen that some new peaks appeared in the fingerprint region with the extension of irradiation time. A closer look at the fingerprint region is shown in Fig. 7c and exhibited the appearance of characteristic absorption peaks associated with the functional groups. More specifically, the bands in the FTIR spectra of the treated solution (after irradiation) at 1558 and 1512 cm^{-1} corresponded to N–H in-plane of amide and C=C stretching vibration, respectively. The peaks at 1543 and 1265 cm^{-1} were both assigned to C–N stretching vibration. In addition, the bands in the range of 2250–2400 cm^{-1} (marked in the red dotted box in Fig. 7b) were attributed to CO_2 [45] and the intensity of characterization bands increased with the prolongation of irradiation time indicating the mineralization of the dye [46]. The FTIR results clearly suggested that the chromophore part of AO7 was destroyed in the MIL-53(Fe)/PS/Vis process, and that the dye molecule underwent

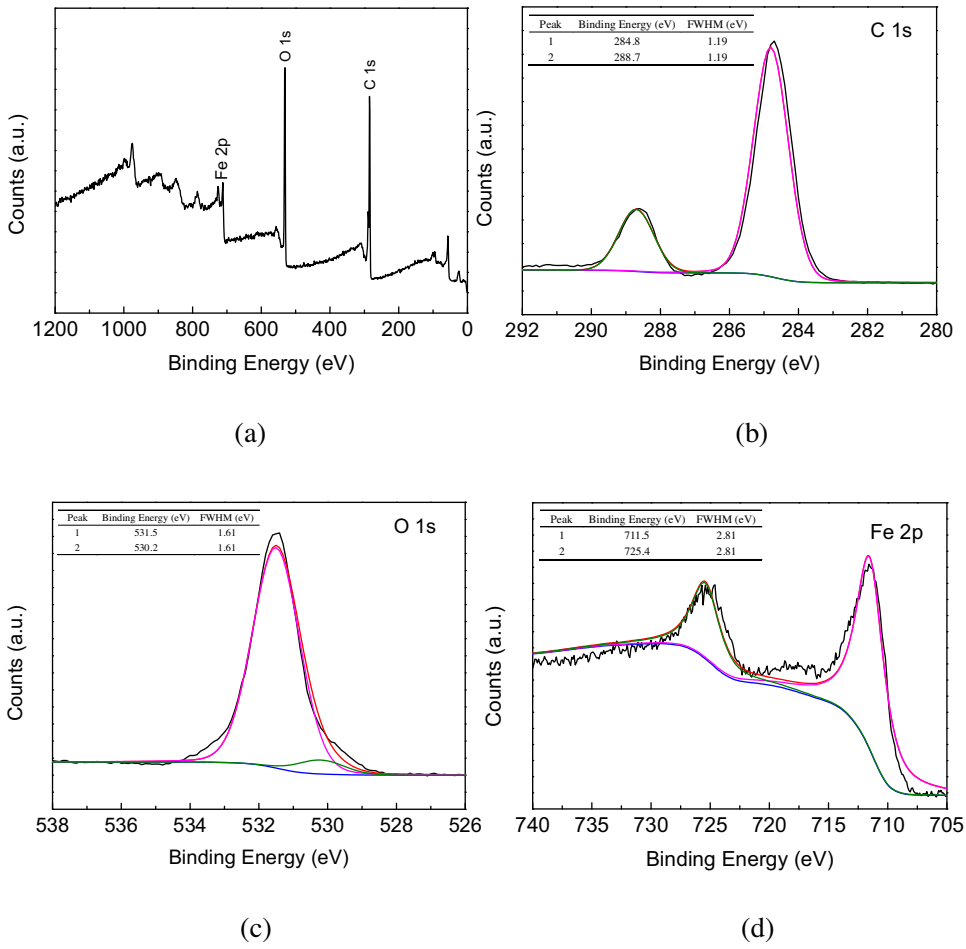

Fig. 4. XPS spectra of MIL-53(Fe): (a) the survey spectrum; (b) high-resolution C 1s; (c) high-resolution O 1s; (d) high-resolution Fe 2p.

irreversible degradation to smaller species and CO_2, consistent with the changes in absorption spectra [47]. However, the principal bands in the FTIR spectrum of AO7 (before irradiation) were not disappeared thoroughly after 90 min of irradiation, implying that more irradiation time might be required for the complete mineralization of the dye.

To identify the key factor responsible for the accelerated photocatalytic degradation of AO7 in the MIL-53(Fe)/PS/Vis process, the photoluminescence (PL) technique was employed to explore the efficiency of the charge carrier trapping, migration and transfer [48,49]. The PL spectra for the photocatalyst suspension in water with and without the addition of PS are shown in Fig. 8a. Upon photoexcitation at 340 nm, the MIL-53(Fe) photocatalyst exhibited a broad band at 400–500 nm with a peak at 465 nm. The energy of the PL peak (2.67 eV) basically agreed with the optical band gap energy (2.62 eV), which was calculated from the UV–vis DRS spectrum of MIL-53(Fe). Since the PL emission mainly originated from the recombination of excited electrons and holes, a weaker intensity of emission peak indicated a lower recombination possibility of photoinduced charge carriers [50]. As a further demonstration, the PL intensity for MIL-53(Fe) suspension in the presence of PS was lower than that for the one in the absence of PS, that is to say, the recombination of photogenerated electrons and holes was inhibited in the presence of PS. This can be interpreted by the fact that the introduced PS, serving as the electron acceptor, could suppress the recombination of photoinduced electrons and holes, thereby accelerating the photocatalytic degradation of AO7 via a radical pathway, where the radicals were predominantly originated from the activation of PS by visible light irradiated MIL-53(Fe).

Apart from the PL spectra, the transient photocurrent responses of MIL-53(Fe) with and without PS in aqueous Na_2SO_4 solution were measured under visible light illumination with several on-off cycles to further support the suppression of the recombination of photogenerated charge carriers by PS. The results in Fig. 8b clearly demonstrated that the introduction of PS significantly reduced the photocurrent density of the MIL-53(Fe)/PS/Vis process in comparison to that of the MIL-53(Fe)/Vis process, which was due to the capability of PS in efficiently trapping the photogenerated electrons, closely consistent with the results presented by the PL spectra. Moreover, the photocurrents of the MIL-53(Fe)/Vis and MIL-53(Fe)/PS/Vis processes were highly repeatable during 14 on-off cycles, indicating good photostability of the MOF-coated photoelectrode.

3.3. Reusability and stability of MIL-53(Fe)

The reusability and stability is a prerequisite for the catalyst to be used in practical applications and therefore the photocatalytic activity of MIL-53(Fe) after repeated use was assessed in five successive AO7 degradation experiments under the identical experimental conditions [51]. As shown in Fig. 9, there was no significant decrease in the degradation of AO7 through each cycle. The MIL-53(Fe) photocatalyst exhibited excellent reusability and maintained a similar photocatalytic activity for more than 450 min, indicating good reusability of this photocatalyst for AO7 degradation. Related to the stability of the metal-based catalysts, absence of leaching of metal species from the solid to aqueous phase is one key issue since this process can afford a minimum concentration of

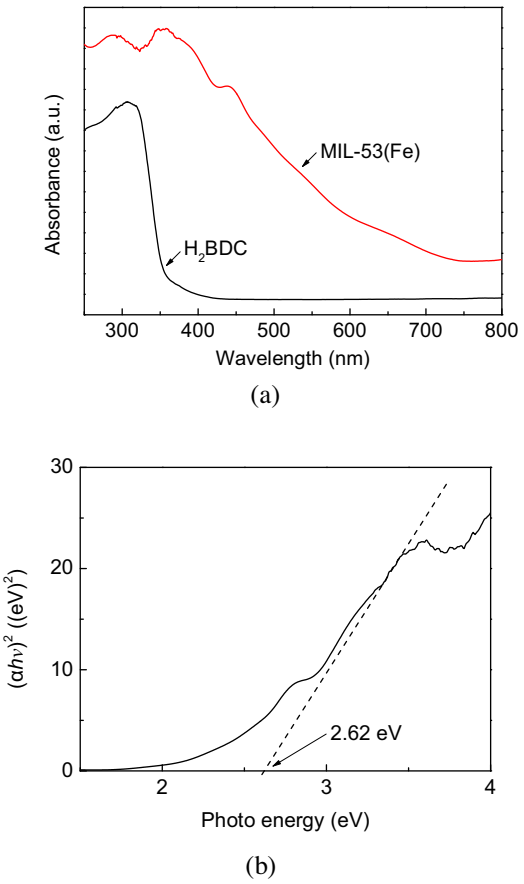

Fig. 5. (a) UV–vis diffuse reflectance spectra of MIL-53(Fe) and H_2BDC; (b) Plot of $(\alpha h\nu)^2$ versus photo energy ($h\nu$) for MIL-53(Fe).

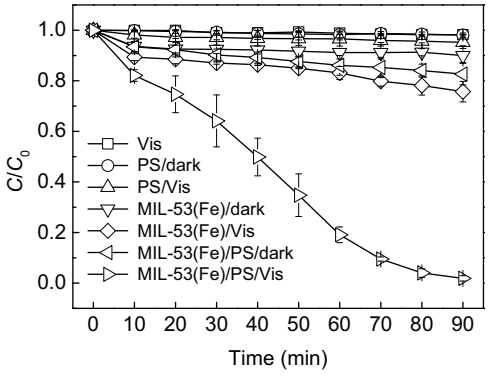

Fig. 6. Variation of AO7 concentration (C/C_0) with reaction time in various catalytic processes. Reaction conditions: AO7 (0.05 mM); MIL-53(Fe) (0.6 g L^{-1}); PS (2.0 mM); initial pH 6.0.

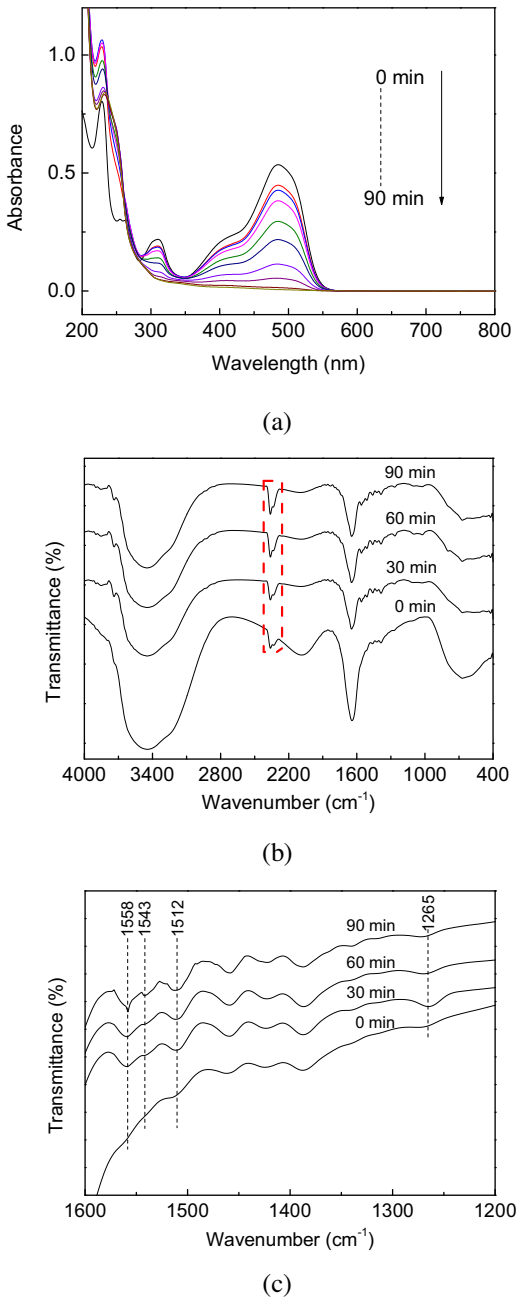

Fig. 7. (a) Representative UV–vis spectra changes during AO7 decolorization by the MIL-53(Fe)/PS/Vis process. Reaction conditions: AO7 (0.05 mM); MIL-53(Fe) (0.6 g L^{-1}); PS (2.0 mM); initial pH 6.0. (b) Temporal variations in the FTIR spectra in the photocatalytic degradation of AO7 under visible light irradiation (the full absorption spectra). Reaction conditions: AO7 (0.05 mM); MIL-53(Fe) (0.6 g L^{-1}); PS (2.0 mM); initial pH 6.0. (c) Temporal variations in the FTIR spectra in the photocatalytic degradation of AO7 under visible light irradiation (the fingerprint region). Reaction conditions: AO7 (0.05 mM); MIL-53(Fe) (0.6 g L^{-1}); PS (2.0 mM); initial pH 6.0.

the metal species in solution that can serve as homogeneous catalyst [52]. In this regard, the amount of leached iron ions after the reaction was measured and it was found that MIL-53(Fe) showed excellent stability with negligible Fe leaching at the normal pH 6.0 (0.37 mg L^{-1}), rendering MIL-53(Fe) a potential candidate for industrial wastewater treatment.

3.4. Mechanism discussion

To better understand the mechanism for the accelerated photocatalytic degradation of AO7 in the MIL-53(Fe)/PS/Vis process, the band structure of MIL-53(Fe) with respect to the redox ability of photoinduced charge carriers was firstly evaluated. A typical Mott-Schottky plot of MIL-53(Fe) measured at a frequency of 100 Hz in the dark is shown in Fig. 10 and the positive slope of the plot revealed an n-type semiconductor feature for the prepared MIL-53(Fe). The flat-band potential extrapolated for MIL-53(Fe) was −0.61 V versus SCE, corresponding to −0.37 V versus normal hydrogen electrode (NHE). For n-type semiconductors, the flat-band potential was 0–0.1 V higher than the conduction-band potential [53]. This means that the conduction-band minimum (CBM) of MIL-53(Fe) was negatively shifted to be −0.47 V versus NHE,

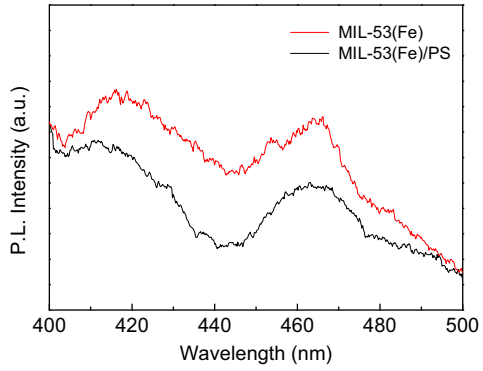

(a)

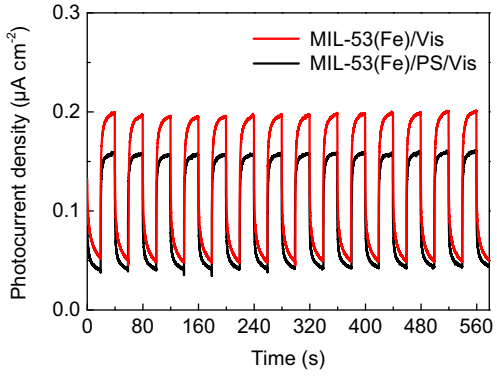

(b)

Fig. 8. (a) Photoluminescence spectra for MIL-53(Fe) suspension with and without the addition of PS. Reaction conditions: MIL-53(Fe) (0.6 g L^{-1}); PS (2.0 mM); initial pH 6.0. (b) Transient photocurrent responses of MIL-53(Fe) with and without the addition of PS measured at the potential of 0.2 V versus SCE under visible LED light irradiation. Reaction conditions: PS (2.0 mM); Na_2SO_4 (0.5 M).

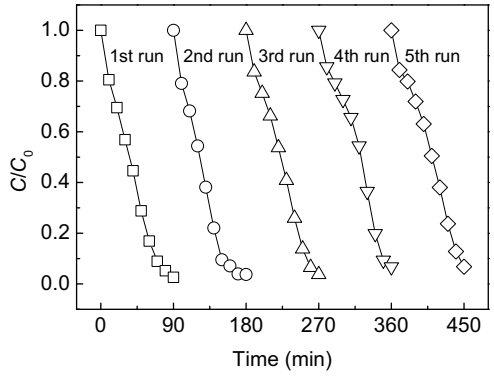

Fig. 9. The reusability of MIL-53(Fe) for the photocatalytic degradation of AO7 under visible LED light mediated by PS. Reaction conditions: AO7 (0.05 mM); MIL-53(Fe) (0.6 g L^{-1}); PS (2.0 mM); initial pH 6.0.

which was more significantly negative than the redox potential of $SO_4^{\bullet-}/S_2O_8^{2-}$ [54], satisfying the thermodynamic requirements for the production of $SO_4^{\bullet-}$ radicals via the activation of PS by photogenerated electrons under visible light irradiation. Combination of the band gap energy derived from UV–vis DRS spectra, the valence-band potential of MIL-53(Fe) was calculated to be 2.15 V versus NHE, being lower than the redox potential of $^{\bullet}OH/OH^-$ (2.38 V versus NHE) and thus indicating that MIL-53(Fe) was unable to oxidize OH^- to $^{\bullet}OH$ radicals through the hole oxidation of

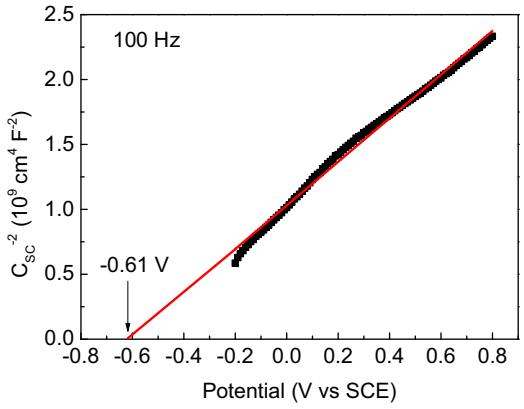

Fig. 10. Mott-Schottky plots of MIL-53(Fe) measured at a frequence of 100 Hz in the dark.

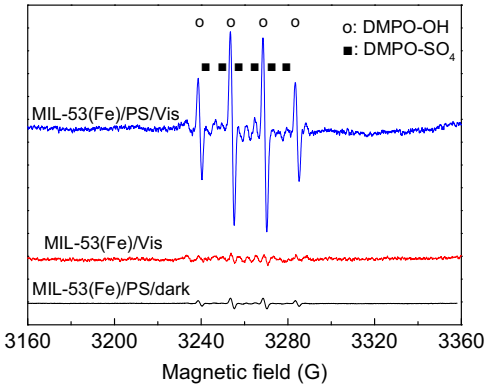

Fig. 11. EPR spectra of various catalytic processes. Reaction conditions: MIL-53(Fe) (0.6 g L^{-1}); PS (2.0 mM); DMPO (18 mM); initial pH 6.0; Reaction time 10 min.

hydroxyl ion [15,54]. However, the valence-band potential of MIL-53(Fe) was more positive than the redox potential of AO7 (1.54 V) [55], suggesting that for photocatalytically degrading AO7 in the MIL-53(Fe)/PS/Vis process direct hole oxidation was thermodynamically permissible.

Furthermore, EPR tests with DMPO as a radical spin trapping agent were performed to support the above speculation. The EPR spectra for various catalytic processes are shown in Fig. 11 and the appearance of very weak signals observed in the MIL-53(Fe)/PS/dark and MIL-53(Fe)/Vis processes indicated that MIL-53(Fe) (i) was not easy to activate PS if not irradiated and (ii) was incapable of oxidizing hydroxyl ion to generate $^{\bullet}OH$ radicals, being supportive of the hole oxidation of AO7 in the irradiated MIL-53(Fe) suspension. When PS and visible light irradiation was simultaneously present, signals of significant intensity for DMPO-SO_4 and DMPO-OH adducts were noticed in the MIL-53(Fe)/PS/Vis process, indicating the formation of $SO_4^{\bullet-}$ and $^{\bullet}OH$ radicals [26,56].

On the basis of above results, a plausible mechanism for the degradation of AO7 over MIL-53(Fe) in the presence of PS under visible light irradiation was proposed (Fig. 12). As previously shown in Fig. 5a, the pure organic linker (H_2BDC) had no optical response in the visible light range, therefore, it is rational to believe that the direct photoexcitation of Fe-oxo cluster upon visible light irradiation was responsible for the photocatalytic activity of MIL-53(Fe) [30,57]. Particularly, MIL-53(Fe) was excited by the action of visible light photons and then the photoinduced electrons and holes were generated accordingly. Due to the presence of PS, the photogenerated electrons could be trapped by PS to produce $SO_4^{\bullet-}$ radicals, effectively facilitating the separation of electrons and holes and

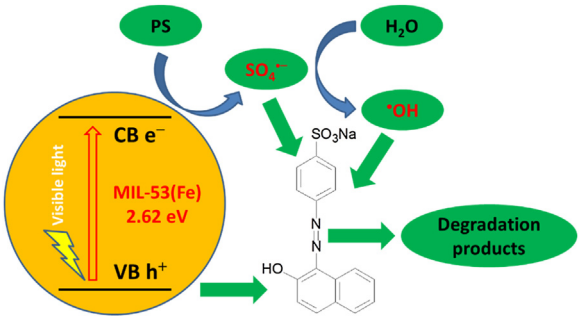

Fig. 12. Plausible mechanism of photocatalytic degradation of AO7 in the MIL-53(Fe)/PS/Vis process.

subsequently the holes with strong oxidation capacity could oxidize AO7 directly. Meanwhile, the presence of $SO_4^{\bullet-}$ radicals in aqueous solution could result in radical interconversion reactions to yield $^{\bullet}OH$ radicals [58], where these two radicals should be held accountable for the accelerated photocatalytic degradation of AO7 in the MIL-53(Fe)/PS/Vis process.

3.5. Effect of several parameters on photocatalytic activity of MIL-53(Fe)

The practical application of the photocatalyst requires a preliminary evaluation of the effect of various operating parameters on the photocatalytic performance and thus the effect of major factors in terms of the amount of photocatalyst, PS concentration and initial pH on the degradation of AO7 in the MIL-53(Fe)/PS/Vis process was investigated [59]. As can be seen from Fig. 13a, an increase in the photocatalyst dosage in the range from 0.1 to 0.6 g L^{-1} resulted in a striking enhancement in the extent of degradation from 36% to 98%. This can be due to the fact that by increasing the photocatalyst dosage, more electrons and holes would be generated as a result of photoexcitation of MIL-53(Fe) upon visible light irradiation and the photogenerated electrons could be captured by PS to increase the amount of $SO_4^{\bullet-}$ radicals, but this was noted only for relatively low dosages. The deleterious effect observed for high amount of catalyst (e.g., 0.8 g L^{-1}) can be attributed to the suspension that would cause a relevant fraction of the incident radiation to be lost via scattering, not being absorbed and therefore no longer being available to induce the photocatalytic process [60,61].

In the PS-mediated photocatalytic process, the PS concentration is directly related to the amount of radicals (i.e., $SO_4^{\bullet-}$ and $^{\bullet}OH$) generated, and thus to the photocatalytic performance achieved. It can be seen from Fig. 13b that when increasing the PS concentration from 1.0 to 2.0 mM, the degradation of AO7 was slightly accelerated due to the formation of more radicals. However, no significant additional enhancement for the degradation of AO7 was observed, but rather decreased a little, when the PS concentration was above 2.0 mM, possibly because scavenging of $SO_4^{\bullet-}$ radicals would occur at higher PS concentration, as expressed by the following equations:

$$SO_4^{\bullet-} + S_2O_8^{2-} \rightarrow S_2O_8^{\bullet-} + SO_4^{2-} \quad (1)$$

$$SO_4^{\bullet-} + SO_4^{\bullet-} \rightarrow S_2O_8^{2-} \quad (2)$$

It is important to remark that $S_2O_8^{\bullet-}$ is less reactive than $SO_4^{\bullet-}$, and hence an increased concentration of PS has a diminishing return on the reaction rate indicating the existence of an optimum oxidant concentration in the oxidation process. In the MIL-53(Fe)/PS/Vis process, the optimum concentration of PS was found to be 2.0 mM, which was close to the theoretical stoichiometric amount of PS (2.1 mM) for complete mineralization of 0.05 mM AO7 according to Eq. (3). In addition, the optimum PS concentration (2.0 mM) was

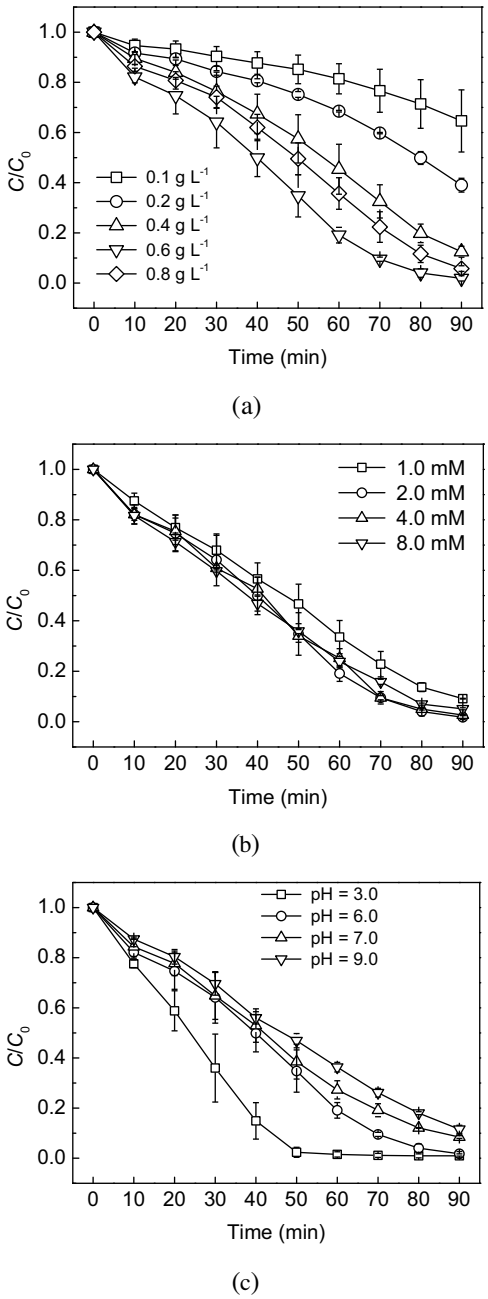

Fig. 13. Effect of several operating parameters on the photocatalytic degradation of AO7 in the MIL-53(Fe)/PS/Vis process: (a) amount of photocatalyst; (b) PS concentration; (c) initial pH. Reaction conditions: (a) AO7 (0.05 mM); PS (2.0 mM); initial pH = 6.0; (b) AO7 (0.05 mM); MIL-53(Fe) (0.6 g L^{-1}); initial pH = 6.0; (c) AO7 (0.05 mM); MIL-53(Fe) (0.6 g L^{-1}); PS (2.0 mM).

quite lower than the corresponding H_2O_2 concentration (20.0 mM) in the MIL-53(Fe)/visible light/H_2O_2 system [23].

$$C_{16}H_{11}N_2NaO_4S + 42\,S_2O_8^{2-} + 38\,H_2O \rightarrow 16CO_2 + 87\,H^+ + Na^+ + 2NO_3^- + 85SO_4^{2-} \quad (3)$$

The pH of the medium is a crucial operating parameter, as it directly influences not only the photocatalytic activity but also the extent of Fe leaching from the catalyst [61]. Fig. 13c shows the effect of initial pH on the degradation of AO7 in the MIL-53(Fe)/PS/Vis process and it was found that the present photocatalytic process worked effectively over a broad pH range from 3.0 to 9.0. However,

the AO7 degradation at pH 3.0 was much more rapid than that of other pH values, which might be relevant to Fe ions leaching from the catalyst to aqueous phase under strong acidic condition. To this end, the concentration of the leached iron as a function of initial solution pH was monitored and the results are shown in Fig. S4 and the high level of leached iron at pH 3.0 (7.53 mg L^{-1}) demonstrated that the homogeneous Fenton-like process could be formed and contribute to the rapid degradation of AO7. However, the concentrations of iron leached from the catalyst in the pH range of 6.0–9.0 were all below 0.37 mg L^{-1} and were negligible from the catalytic perspective, indicating that MIL-53(Fe) exhibited a reasonable good stability under neutral or basic conditions. In addition, the treatment of wastewaters without pre-adjusting their pH might also become feasible, since industrial organic contaminated wastewaters often have pH around 7.0 [62].

4. Conclusions

A visible-light-responsive photocatalyst, namely MIL-53(Fe), has been synthesized successfully by a facile hydrothermal process and employed for photocatalytic degradation of an organic dye from aqueous solution under visible LED light irradiation. MIL-53(Fe) can degrade AO7 via the direct hole oxidation pathway under visible light illumination but with an unsatisfactory degradation efficiency. The introduction of PS at a low stoichiometric concentration can significantly accelerate the photocatalytic degradation of AO7 in the MIL-53(Fe)/PS/Vis process. The results of PL spectra and electrochemical measurements together with EPR analysis revealed that the introduced PS could suppress the recombination of photoinduced electrons and holes and thus increase the production of reactive radicals through the activation of PS by photogenerated electrons, thereby accelerating the photocatalytic degradation of AO7. Moreover, the MIL-53(Fe) photocatalyst showed reasonable good reusability and stability with a low level of iron leaching under near-neutral condition. It is anticipated that this study could provide a new near-neutral persulfate-mediated photocatalytic process for pollutant control and widen the application range of MOFs as photocatalysts.

Acknowledgements

This work was supported by Natural Science Foundation of Hubei Province (Grant No. 2012FFA089), Natural Science Foundation of China (Grant No. 21547006), Wuhan Applied Basic Research Project (Grant No. 2016060101010074) and Shenzhen Basic Research Plan Project (Grant No. JCYJ20150508152951667). The analyses of XRD, FESEM, EDS and XPS were partially supported by Large-scale Instrument and Equipment Sharing Foundation of Wuhan University.

Appendix A. Supplementary data

Supplementary data associated with this article can be found, in the online version, at http://dx.doi.org/10.1016/j.apcatb.2016.09.005.

References

[1] T. Zhang, W. Lin, Chem. Soc. Rev. 43 (2014) 5982–5993.
[2] K. Villa, S. Murcia-López, T. Andreu, J.R. Morante, Appl. Catal. B: Environ. 163 (2015) 150–155.
[3] S. Cao, C.J. Wang, X.J. Lv, Y. Chen, W.F. Fu, Appl. Catal. B: Environ. 162 (2015) 381–391.
[4] T. Baran, S. Wojtyła, A. Dibenedetto, M. Aresta, W. Macyk, Appl. Catal. B: Environ. 178 (2015) 170–176.
[5] C.C. Wang, J.R. Li, X.L. Lv, Y.Q. Zhang, G. Guo, Energy Environ. Sci. 7 (2014) 2831–2867.
[6] D. Wang, R. Huang, W. Liu, D. Sun, Z. Li, ACS Catal. 4 (2014) 4254–4260.
[7] Y. Bai, G.J. He, Y.G. Zhao, C.Y. Duan, D.B. Dang, Q.J. Meng, Chem. Commun. 14 (2006) 1530–1532.
[8] L.J. Murray, M. Dincă, J.R. Long, Chem. Soc. Rev. 38 (2009) 1294–1314.
[9] L.J. Rong, R.J. Kuppler, Z.H. Cai, Chem. Soc. Rev. 38 (2009) 1477–1504.
[10] J. Lee, O.K. Farha, J. Roberts, K.A. Scheidt, S.T. Nguyen, J.T. Hupp, Chem. Soc. Rev. 38 (2009) 1450–1459.
[11] C.G. Silva, A. Corma, H. Garcia, J. Mater. Chem. 20 (2010) 3141–3156.
[12] F.X. Llabrés i Xamena, A. Corma, H. Garcia, J. Phys. Chem. C 111 (2007) 80–85.
[13] M.C. Das, H. Xu, Z. Wang, G. Srinivas, W. Zhou, Y.F. Yue, V.N. Nesterov, G. Qian, B. Chen, Chem. Commun. 47 (2011) 11715–11717.
[14] L. Shen, W. Wu, R. Liang, R. Lin, L. Wu, Nanoscale 5 (2013) 9374–9382.
[15] C. Zhang, L. Ai, J. Jiang, Ind. Eng. Chem. Res. 54 (2015) 153–163.
[16] H. Li, Y. Zhou, W. Tu, J. Ye, Z. Zou, Adv. Funct. Mater. 25 (2015) 998–1013.
[17] C. Wang, K.E. deKrafft, W. Lin, J. Am. Chem. Soc. 134 (2012) 7211–7214.
[18] W. Zhu, P. Liu, S. Xiao, W. Wang, D. Zhang, H. Li, Appl. Catal. B: Environ. 172–173 (2015) 46–51.
[19] P. Shukla, I. Fatimah, S. Wang, H.M. Ang, M.O. Tadé, Catal. Today 157 (2010) 410–414.
[20] H. Sun, S. Liu, S. Liu, S. Wang, Appl. Catal. B: Environ. 146 (2014) 162–168.
[21] L. Duan, B. Sun, M. Wei, S. Luo, F. Pan, A. Xu, X. Li, J. Hazard. Mater. 285 (2015) 356–365.
[22] J.J. Du, Y.P. Yuan, J.X. Sun, F.M. Peng, X. Jiang, L.G. Qiu, A.J. Xie, Y.H. Shen, J.F. Zhu, J. Hazard. Mater. 190 (2011) 945–951.
[23] L. Ai, C. Zhang, L. Li, J. Jiang, Appl. Catal. B: Environ. 148–149 (2014) 191–200.
[24] C. Serre, F. Millange, C. Thouvenot, M. Noguès, G. Marsolier, D. Louër, G. Férey, J. Am. Chem. Soc. 124 (2002) 13519–13526.
[25] K. Zhao, X. Zhang, L. Zhang, Electrochem. Commun. 11 (2009) 612–615.
[26] Y. Gao, Z. Zhang, S. Li, J. Liu, L. Yao, Y. Li, H. Zhang, Appl. Catal. B: Environ. 185 (2016) 22–30.
[27] N. Wahba, M. El Asmar, M. El Sadr, Anal. Chem. 31 (1959) 1870–1871.
[28] National general administration of environmental protection, in: Water Quality-Determination of Iron-Phenanthroline Spectrophotometry (HJ/T 345-2007), Environmental Science Press Of China, Beijing, 2007 (in Chinese).
[29] F. Millange, N. Guillou, R.I. Walton, J.M. Grenèche, I. Margiolaki, G. Férey, Chem. Commun. 473 (2008) 2–4734.
[30] R. Liang, F. Jing, L. Shen, N. Qin, L. Wu, J. Hazard. Mater. 287 (2015) 364–372.
[31] P. Horcajada, C. Serre, G. Maurin, N.A. Ramsahye, F. Balas, M. Vallet-Regi, M. Sebban, F. Taulelle, G. Férey, J. Am. Chem. Soc. 130 (2008) 6774–6780.
[32] A. Banerjee, R. Gokhale, S. Bhatnagar, J. Jog, M. Bhardwaj, B. Lefez, B. Hannoyer, S. Ogale, J. Mater. Chem. 22 (2012) 19694–19699.
[33] C. Gong, D. Chen, X. Jiao, Q. Wang, J. Mater. Chem. 12 (2002) 1844–1847.
[34] C. Zhang, L. Ai, J. Jiang, J. Mater. Chem. A 3 (2015) 3074–3081.
[35] S.K. Tam, J. Dusseault, S. Polizu, M. Ménard, J.P. Hallé, L.H. Yahia, Biomaterials 26 (2005) 6950–6961.
[36] V. Chandra, J. Park, Y. Chun, J.W. Lee, I.C. Hwang, K.S. Kim, ACS Nano 4 (2010) 3979–3986.
[37] G.T. Vuong, M.H. Pham, T.O. Do, CrystEngComm 15 (2013) 9694–9703.
[38] G.T. Vuong, M.H. Pham, T.O. Do, Dalton Trans. 42 (2012) 550–557.
[39] X.J. Chen, Y.Z. Dai, X.Y. Wang, J. Guo, T.H. Liu, F.F. Li, J. Hazard. Mater. 292 (2015) 9–18.
[40] C.H. Hendon, D. Tiana, M. Fontecave, C.M. Sanchez, L. D'arras, C. Sassoye, L. Rozes, C. Mellot-Draznieks, A. Walsh, J. Am. Chem. Soc. 135 (2013) 10942–10945.
[41] L. Qin, Z. Li, Z. Xu, X. Guo, G. Zhang, Appl. Catal. B: Environ. 179 (2015) 500–508.
[42] H. Li, Y. Gong, Q. Huang, H. Zhang, Ind. Eng. Chem. Res. 52 (2013) 15560–15567.
[43] P. Ji, J. Zhang, F. Chen, M. Anpo, Appl. Catal. B: Environ. 85 (2009) 148–154.
[44] J. Wu, H. Zhang, J. Qiu, J. Hazard. Mater. 215–216 (2012) 138–145.
[45] W.C. Wu, L.F. Liao, C.F. Lien, J.L. Lin, Phys. Chem. Chem. Phys. 3 (2001) 4456–4461.
[46] Y. Shen, L. Wang, Y. Wu, X. Li, Q. Zhao, Y. Hou, W. Teng, Catal. Commun. 68 (2015) 11–14.
[47] J. Li, W. Ma, Y. Huang, X. Tao, J. Zhao, Y. Xu, Appl. Catal. B: Environ. 48 (2004) 17–24.
[48] S.C. Yan, Z.S. Li, Z.G. Zou, Langmuir 26 (2010) 3894–3901.
[49] Y. Huang, W. Fan, B. Long, H. Li, F. Zhao, Z. Liu, Y. Tong, H. Ji, Appl. Catal. B: Environ. 185 (2016) 68–76.
[50] Y. Yang, J. Wen, J. Wei, R. Xiong, J. Shi, C. Pan, ACS Appl. Mater. Inter. 5 (2013) 6201–6207.
[51] Y. Yao, Y. Cai, F. Lu, J. Qin, F. Wei, C. Xu, S. Wang, Ind. Eng. Chem. Res. 53 (2014) 17294–17302.
[52] S. Navalon, M. Alvaro, H. Garcia, Appl. Catal. B: Environ. 99 (2010) 1–26.
[53] J. Huang, Q. Shang, Y. Huang, F. Tang, Q. Zhang, Q. Liu, S. Jiang, F. Hu, W. Liu, Y. Luo, T. Yao, Y. Jiang, Z. Pan, Z. Sun, S. Wei, Angew. Chem. Int. Ed. 54 (2015) 1–6.
[54] G. Zhou, H. Sun, S. Wang, H.M. Ang, M.O. Tadé, Sep. Purif. Technol. 80 (2011) 626–634.
[55] X. Chen, X. Qiao, D. Wang, J. Lin, J. Chen, Chemosphere 67 (2007) 802–808.

[56] C. Tan, N. Gao, Y. Deng, J. Deng, S. Zhou, J. Li, X. Xin, J. Hazard. Mater. 276 (2014) 452–460.
[57] K.G. Laurier, F. Vermoortele, R. Ameloot, D.E. De Vos, J. Hofkens, M.B. Roeffaers, J. Am. Chem. Soc. 135 (2013) 14488–14491.
[58] C. Liang, Z.S. Wang, C.J. Bruell, Chemosphere 66 (2007) 106–113.
[59] S. Luo, L. Duan, B. Sun, M. Wei, X. Li, A. Xu, Appl. Catal. B: Environ. 164 (2015) 92–99.
[60] B. Iurascu, I. Siminiceanu, D. Vione, M. Vicente, A. Gil, Water Res. 43 (2009) 1313–1322.
[61] J. Herney-Ramirez, M.A. Vicente, L.M. Madeira, Appl. Catal. B: Environ. 98 (2010) 10–26.
[62] A.C.K. Yip, F.L.Y. Lam, X. Hu, Ind. Eng. Chem. Res. 44 (2005) 7983–7990.